Reconstruction of the 3D flow field in a differentially heated rotating annulus by synchronized particle image velocimetry and infrared thermography measurements

Uwe Harlander[1], Grady B. Wright[2], Christoph Egbers[1]

1: Dept. of Aerodynamics and Fluid Mechanics, BTU Cottbus, Germany,
2: Department of Mathematics, Boise State University, Boise, USA
[*]Correspondent author: haruwe@tu-cottbus.de

Keywords: PIV/LDA processing, infrared thermography, baroclinic instability, radial basis functions

Introduction

In the earth's atmosphere baroclinic instability is responsible for the heat and momentum transport from low to high latitudes. Baroclinic instability leads to the growth of multi-scale vortices that accomplish the meridional heat transport. Raymond Hide used a rather simple laboratory experiment to study such vortices in the lab (Hide, 1953). The experiment is comprised by a cooled inner and heated outer cylinder mounted on a rotating platform, which mimics the heated tropical and cooled polar regions of the earth's atmosphere. The working fluid is water, though recent experiments have also been carried out using air. The experiment shows rich dynamics that have been studied by varying the radial temperature difference and the rate of annulus revolution **w**. Keeping the temperature gradient fixed, an azimuthally symmetric flow regime can be found for small **w.** By increasing **w,** the flow transitions to a wavy regime that becomes chaotic for large **w.**
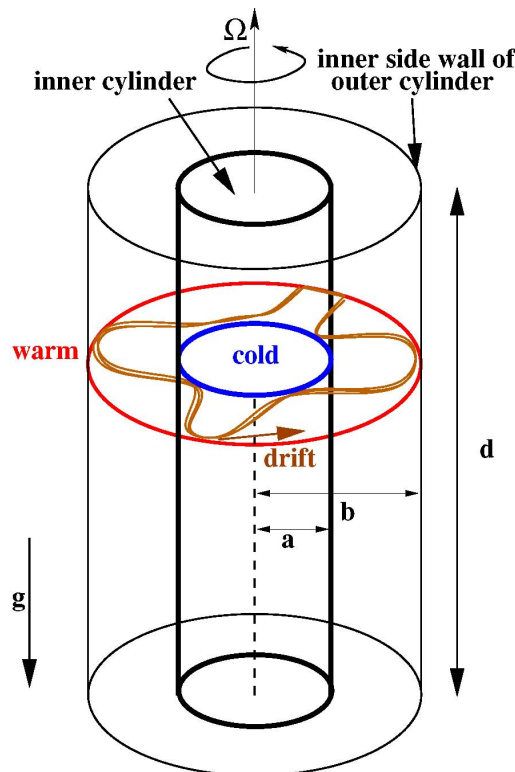
To first order, the transition regime and the spatial patterns of the unstable modes can be described by a linear model formulated by the British meteorologist Eric Eady and referred to as the 'Eady model of baroclinic instability' (Eady, 1949). However, the convective flow in the annulus is more complicated than this simple linear and inviscid model can predict since nonlinearities and boundary layers have a significant impact on the flow. The 3D structure of the annulus flow field has been numerically simulated (e.g. Randriamampianina et al., 2006) but, to our knowledge, has not been measured in the laboratory.

At the Brandenburg University of Technology (BTU) Cottbus the differentially heated rotating annulus is a reference experiment of the DFG priority program 'MetStröm'. The flow is measured by using particle image velocimetry (PIV) and infrared thermography (IRT). In a series of papers (Harlander et al., 2011a,b; Seelig et al., 2011) we investigated the time-spatial behaviour of the experiment by applying multivariate statistical techniques to the data. In the present paper we use novel interpolation techniques to reconstruct the 3D flow field from synchronous PIV and IRT measurements.

Experimental setup

The set-up (see Fig. 1), described in more detail by von Larcher and Egbers (2005), consists of a tank with three concentric cylinders mounted on a turntable. The inner cylinder is made of anodised aluminium and cooled by a thermostat and the middle and outer cylinders are made of borosilicate glass. The outer side-wall of the experiment gap is heated by a heating coil that is mounted at the bottom of the outer cylinder bath. In our setup, the experiment has a flat bottom and free surface. Deionised water is used as the working fluid.
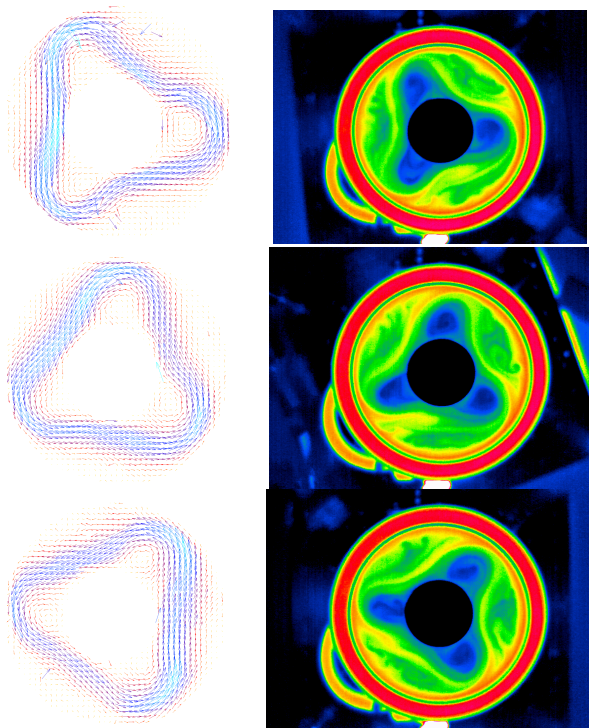
While the most important dynamic parameters (the rotation rate of the annulus, and the temperature difference in the cylindrical gap) are captured by the Taylor number and thermal Rossby number, the physical properties of the working fluid are captured by the Prandtl number.
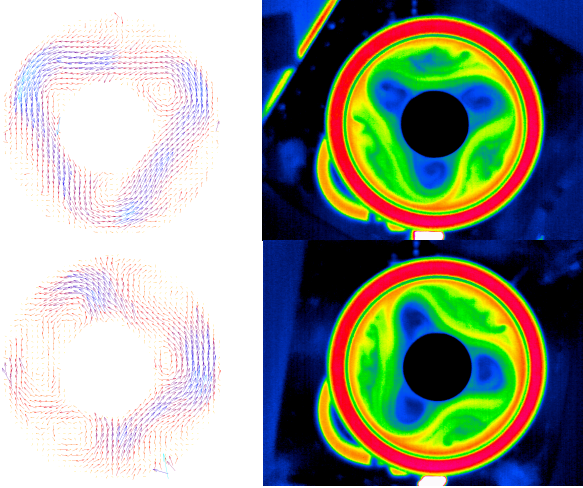
Figure 1*: Sketch of the experiment. Inner radius a=45mm, outer radius b=120mm, height d=135mm.*

Synchronized PIV and IR measurements

A DANTEC Particle Image Velocimetry (PIV) system (see Appendix for technical details) is used to measure the horizontal velocity components at 40, 60, 80, 100, and 120 mm above the bottom. The uppermost level is thus 15 mm below the fluid's surface. The surface temperature is simultaneously measured by an infrared camera (see the Appendix for technical details). The PIV and infrared came-

*Figure 2: Left column: PIV observations at z=120, 100, 80, 60, 40mm from the bottom at time instances t=0, 68, 138, 207, 275s. Right column: Simultaneous surface temperature observations. In the experiment the annulus rotates with **w**=5.02 RPM, the radial temperature difference is dT=6.7K, and the total height of the fluid in the annulus is d=135mm.*

ras have been mounted above the annulus and they co-rotate with the annulus.

From the PIV observations alone a coherent 3D picture of the flow cannot be constructed since the PIV measurements have been taken at different instants of time. Therefore a corresponding IR image has been recorded for each PIV measurement. These IR images can be used to reconstruct the correct phase of the measured velocity fields. Fig. 2 (left column) shows PIV observations at z=120, 100, 80, 60, 40mm from the bottom at time instances t=0, 68, 138, 207, 275s. In the right column we see the corresponding surface temperatures. Each IR and PIV image for which t>0 is rotated back to the position at t=0. Then all waves shown in blue in the IR images have the same phase as the wave in the upper right picture of Fig. 2. In contrast, the PIV velocity fields generally have different phases since they have been taken at different vertical levels. From these rotated fields, a 3D flow field can be reconstructed that is an approximation to the true 3D flow.

The basis for this approximation was given already by G. I. Taylor (1938). There he deduced the spatial fluctuations of a turbulent velocity from the corresponding measurements of temporal fluctuations at a single point. Today this hypothesis is known as Taylor's frozen-flow hypothesis. Here we apply this hypothesis to a slowly evolving quasigeostrophic flow. Harlander et al. (2009) has demonstrated that this works well for such flows by constructing 2D horizontal velocity fields from 1D observations in time.

In the following we show how the 3D velocity field is obtained from the vertically stacked horizontal velocity fields.

Data Analysis

The first step in reconstructing the full 3D velocity field is to reconstruct the horizontal velocity fields at each of the five vertical levels where the velocity fields have been measured. The PIV measurements of these horizontal velocity fields do not line up on a nice grid. We therefore use a mesh-free reconstruction method based on radial basis functions (RBFs). The method we use employs matrix-valued RBFs (Narcowich and Ward 1994) and mimics the Helmholtz decomposition of a 2D velocity field. It is similar to the method described in Fuselier and Wright (2009) for the surface of the sphere, but is instead adapted for a 2D annular domain. Additionally, we employ a filtering strategy for dealing with the noise in the measured velocity fields.

Let $\mathbf{u}_j^{(\ell)} = \left(u_j^{(\ell)}, v_j^{(\ell)} \right), j = 1, \ldots, N^{(\ell)}$ denote the normalized measurements of the horizontal velocity field at level ℓ and $\mathbf{x}_j = (x_j, y_j)$ denote the corresponding normalized locations of the measured field. Here we have normalized so that the outer radius of the tank is one. The matrix-valued RBF approximation to these measurements takes the form

$$\tilde{\mathbf{u}}^{(\ell)}(\mathbf{x}) = \sum_{j=1}^{N^{(\ell)}} \left[a\Phi_{div}(\mathbf{x}, \mathbf{x}_j) + (1-a)\Phi_{curl}(\mathbf{x}, \mathbf{x}_j) \right] \mathbf{c}_j^{(\ell)},$$

where $0 \le a \le 1$ and $\mathbf{c}_j^{(\ell)} = \left[c_j^{(\ell)} \; d_j^{(\ell)} \right]^T$. Φ_{div} and Φ_{curl} are matrix-valued kernels and are defined by

$$\Phi_{div}(\mathbf{x},\mathbf{x}_j) = (-\nabla^2 I + \nabla\nabla^T)\phi\left(\left\|\mathbf{x}-\mathbf{x}_j\right\|_2\right),$$

$$\Phi_{curl}(\mathbf{x},\mathbf{x}_j) = -\nabla\nabla^T\phi\left(\left\|\mathbf{x}-\mathbf{x}_j\right\|_2\right),$$

where I is the 2-by-2 identity matrix, $\nabla\nabla^T$ is the Hessian matrix, and ϕ is a (scalar-valued) radial kernel. A simple calculation shows that the columns of Φ_{div} are *divergence- free* and the columns of Φ_{curl} are *curl-free*. Thus, $\tilde{\mathbf{u}}^{(\ell)}(\mathbf{x})$ mimics the Helmholtz decomposition of a 2D vector field (provided $0 < a < 1$).

For this study we use the Matern class of radial kernels in the formulas for Φ_{div} and Φ_{curl}. These are defined by

$$\phi_\nu(r) = \frac{1}{2^{\nu+1}\Gamma(\nu+1)}(\alpha r)^\nu K_\nu(\alpha r),$$

where $\nu > \frac{5}{2}$, $\alpha > 0$, and K_ν is the modified Bessel function of the second kind. This class of kernels is particular popular for spatial statistics (Stein 1999).

To determine the coefficients $\mathbf{c}_j^{(\ell)}$ in the approximations $\tilde{\mathbf{u}}^{(\ell)}(\mathbf{x})$, we set $a = 0.5, \nu = 3.5, \alpha = 20.91$, and enforce the interpolation constraints

$$\tilde{\mathbf{u}}^{(\ell)}(\mathbf{x}_j) = \mathbf{u}_j^{(\ell)}, j = 1,\ldots,N^{(\ell)}.$$
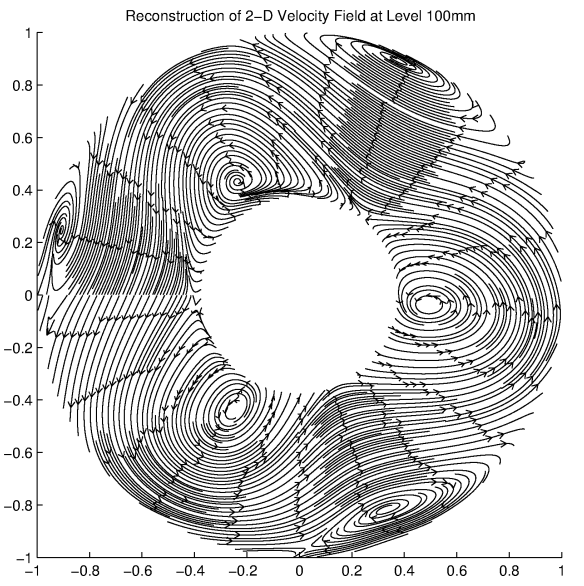
This value of α corresponds to the inverse of the minimum of the pairwise distances between sample locations. The value of ν was selected for smoothness purposes.

We filter the noise from the velocity field reconstructions by adapting a technique first proposed by Beatson and Bui (2007) for scalar-valued RBF approximations. The method involves simply replacing the radial kernel ϕ_ν with a smoother version of itself when *evaluating* the approximations $\tilde{\mathbf{u}}^{(\ell)}(\mathbf{x})$. In all of our reconstructions, we replace the $\nu = 3.5$ Matern radial kernel with the smoother $\nu = 6.5$ kernel. As discussed in Beatson and Bui (2007) this kernel replacement technique corresponds to applying a low-pass filter to the approximations.
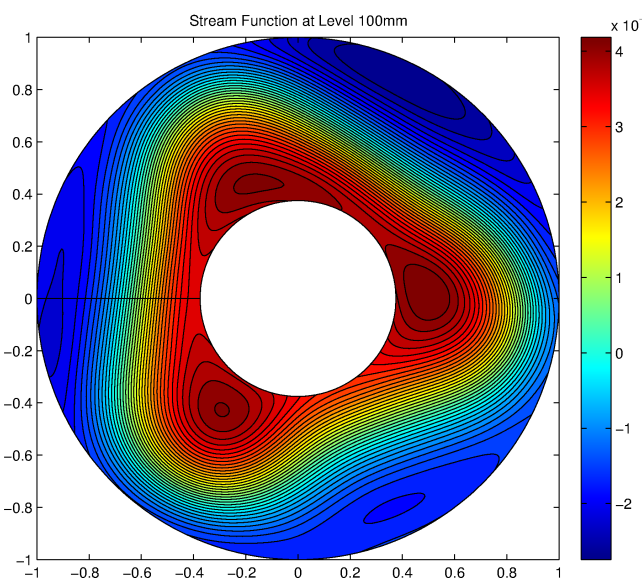
One of the benefits of the matrix-valued RBF reconstruction is that by setting $a = 1$ we can obtain an approximation to the divergence-free portion of the field and similarly by setting $a = 0$ we can obtain an approximation to the curl-free portion. The decomposition into divergence- and curl-free components is important to discriminate different wave types occurring in the annulus. Baroclinic waves and Rossby waves are divergence-free whereas inertia-gravity waves comprise a significant part of horizontal divergence. Presently, the process of spontaneous gravity wave emission is a major issue in atmospheric research. The differentially heated rotating annulus is a lab experiment suitable to systematically study spontaneous gravity wave emission in analogy to the atmosphere (Williams et al., 2008). To detect inertial-gravity waves in the experimental data it is favourable to not use the full flow field but instead make use of the decomposition and analyze just the curl-free part of the flow.

Results
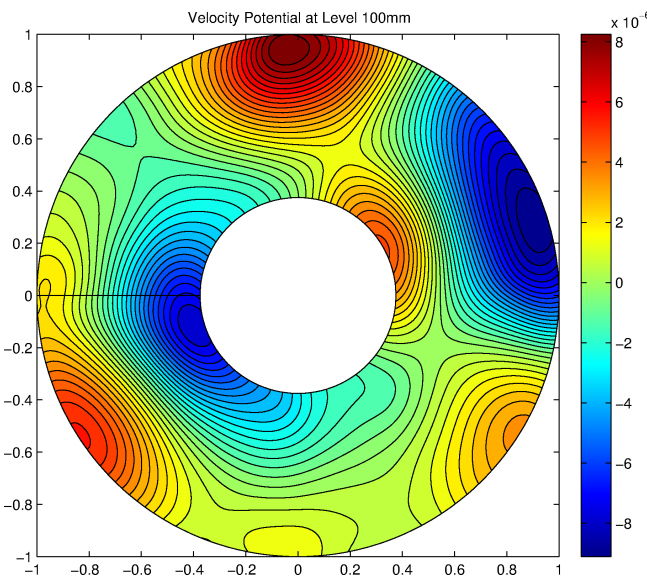
Figure 3(a) shows the streamlines from the matrix-valued RBF reconstruction at the z=100mm level with $a = \frac{1}{2}$. Figure 3(b) shows a contour plot of the stream-function for the divergence-free part of the 100mm field, while 3(c) shows contours of the velocity potential for the curl-free part of the field. As can be seen, the main pattern of the flow is described well by the divergence-free part. This is what we expect since the flow is approximately governed by

(a)

(b)

(c)

Figure 3: *(a) Reconstruction of the velocity field from the PIV data at z=100mm using the matrix-valued RBF method. (b) Stream function and (c) velocity potential for the velocity field from part (a).*

quasigeostrophic dynamics which is divergence-free. The curl-free pattern shown in Figure 3(c) can be interpreted as a deviation from pure quasigeostrophic flow. We see that these deviations are strongest at the inner and outer boundaries of the annulus. There prominent axial flows can be expected due to the heating and cooling of the boundaries. The axial gradients of this flow component induce a horizontal divergence. While the divergence-free part shown in Figure 3(b) is rather robust, the curl-free part is more delicate and already small effects can perturb the symmetry of the pattern. Still, the curl-free part is rather smooth and no small-scale wave like features can be seen. The reason for this might be that the meandering flow shown in Figure 2 does not comprise much transience and thus is in good quasigeostrophic balance. The situation can change for larger Taylor numbers for which the flow becomes more irregular.

To reconstruct each of the vertical components $\tilde{w}^{(\ell)}(\mathbf{x})$ of the full 3D velocity field, we use the continuity equation. Formally, the vertical component at level $\ell = 1, \ldots, 5$ can be written as
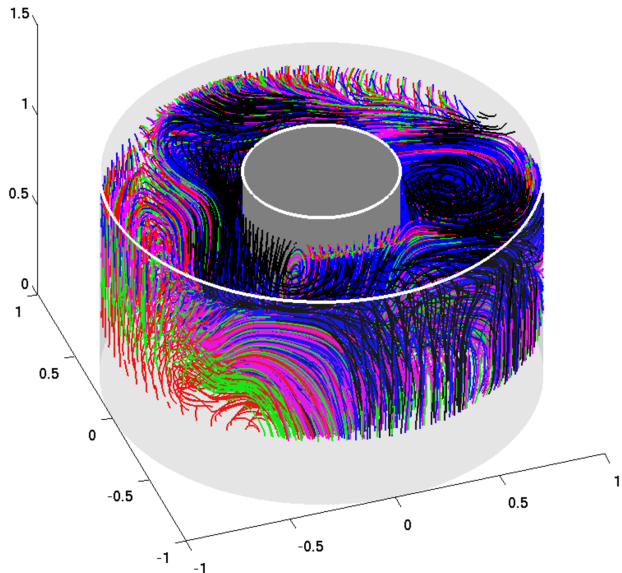
$$\tilde{w}^{(\ell)}(\mathbf{x}) = \tilde{w}^{(\ell-1)}(\mathbf{x}) + \int_{z^{(\ell-1)}}^{z^{(\ell)}} \left[\partial_x \tilde{u}(\mathbf{x}) + \partial_y \tilde{v}(\mathbf{x}) \right] dz .$$

We approximate this value as follows. First, the bottom of the annulus is flat and therefore the vertical velocity there is zero. We denote the vertical velocity at the bottom of the tank by $\tilde{w}^{(0)}(\mathbf{x}) = 0$. To approximate the integral of the horizontal divergence, we use trapezoidal rule. This requires computing the horizontal divergence of the field at each level. We compute this term analytically by differentiating the matrix-valued RBF approximations. For $\ell = 1$, we need the horizontal divergence at level $z=0$. We obtain this value by linearly extrapolating the horizontal divergence from level $\ell = 1$ (40mm) and $\ell = 2$ (60mm).

Figure 4 shows streamlines from the full 3D reconstruction of the velocity field for values between the 40mm and 120mm level. To visualize the streamlines, "particles" have been released at different levels: red at 40mm, green at 60mm, magenta at 80mm, blue at 100 mm, and black at 120mm. As expected from Figure 3(c), we find a strong up- and downdraft at the inner and outer boundary of the annulus. Roughly speaking, due to the spiral flow of the baroclinic wave field, all colours can be found at all vertical levels. Note that the baroclinic tilt of the wave number three pattern with respect to the axial direction is weak. This confirms our conjecture that baroclinic instability is suppressed by non-linear saturation of the flow. Thus the flow is very stable and shows almost no transience.

Conclusion

We have demonstrated that the 3D flow field in a differentially heated rotating annulus can be reconstructed by synchronous PIV and IRT measurements. The method proposed is rather general and can be applied to any convective flow in a cylindrical cavity. Due to shadow effects, reflections or refraction at curved surfaces, PIV data are rarely distributed on a regular grid. Therefore we used a


Figure 4: *Reconstruction of the 3D velocity field from the PIV data from z=40mm to z=120mm. Figure shows individual streamlines of the velocity field seeded at different vertical levels of the cylindrical tank. The colors of the streamlines correspond to the vertical levels of the seeds with red=40mm, green=60mm, magenta=80mm, blue=100mm, black=120mm.*

mesh-free interpolation and reconstruction technique that is based on RBFs. The method is not only suitable for interpolation and filtering but provides also a Helmholtz decomposition of a 2D velocity field into divergence-free and curl-free components. Such a decomposition can be exploited to detect inertial-gravity waves in the flow. For the present dataset no signal of inertial-gravity waves have been found. The 3D reconstruction suggests that the flow is in equilibrium since the baroclinic tilt of the wave is strongly reduced. In the future we will study whether inertial-gravity waves can be found in more transient flows at higher Taylor numbers. Even for highly transient flows the method proposed is appropriate on the condition that the PIV observations at different levels can be taken shortly after each other.

Appendix

A DANTEC Particle Image Velocimetry (PIV) system with a ND:YAG double pulse laser, Litron NANO-L-200-15 PIV, has been used. The output energy of this laser is 200 mJ at 532 nm, with a repetition rate of 15Hz. Pictures have been taken by a FlowSense 2M PIV camera with 1600x1200 pixel and 10 Bit resolution.

The surface temperature has been measured with the infrared camera VarioCam by InfraTec that has a non-cooled microbolometer detector with a spectral range of 7.5-14 μm. The spatial resolution of the sensor is 640x480 pixel. The camera's temperature resolution at 30°C is smaller than 0,08 K with an accuracy of ± 1.5 K. The repetition rate of the system is 50/60 Hz.

Acknowledgements

References

R.K. Beatson and H.-Q Bui (2007), Mollification formulas and implicit smoothing. *Adv. Comput. Math., 27*, 125-149.

E.T. Eady (1949), Long waves and cyclone waves, *Tellus, 1*, 33-52.

E.J. Fuselier and G.B. Wright (2009), Stability and error estimates for vector field interpolation and decomposition on the sphere with RBFs. *SIAM J. Numer. Anal.*, **47**, 3213-3239.

U. Harlander, Th. v.Larcher, Y. Wang, and C. Egbers (2011), PIV- and LDV-measurements of baroclinic wave interactions in a thermally driven rotating annulus. *Exp. Fluids*, **51**, 37-49, doi:10.1007/s00348-009-0792-5, 2011.

U. Harlander, J. Wenzel, Y. Wang, K. Alexandrov, and C. Egbers (2012), Simultaneous PIV- and thermography-measurements of partially blocked flow in a heated rotating annulus. Exp. Fluids, **52**, 1077–1087, doi:10.1007/s00348-011-1195-y.

U. Harlander, H. Ridderinkhof, M.W. Schouten, and W.P.M. De Ruijter (2009), Long term observations of transport, eddies, and Rossby waves in the Mozambique Channel. *J. Geophys. Res*., **114**, C02003, doi:10.1029/2008JC004846

R. Hide (1953), Some experiments on thermal convection in a rotating liquid. *Q. J. R. Met. Soc.*, **79**, 161.

F. J. Narcowich and J. D. Ward (1994), Generalized Hermite interpolation via matrix-valued conditionally positive definite functions. *Math. Comp.*, **63**, 661–687, 1994.

A. Randriamampianina, W.-G. Früh, P.L. Read, and P. Maubert (2006) DNS of bifurcations in an air-filled rotating baroclinic annulus, *J. Fluid Mech.*, **561**, 359-389.

Th. v. Larcher, C. Egbers (2005), Experiments on transitions of baroclinic waves in a differentially heated rotating annulus. *Nonl. Proc. Geophys.*, **12**, 1033–1041.

T. Seelig, U. Harlander, R. Faulwetter, and C. Egbers (2012), Irregularity and singular vector growth in the differentially heated rotating annulus. Theoret. Comp. Fluid Dynamics, published online, doi:10.1007/s00162-011-0255-5.

M. L. Stein (1999), *Interpolation of Spatial Data: Some Theory for Kriging.* Springer-Verlag, New York.

G.I. Taylor (1938), The Spectrum of Turbulence. *Proc. R. Soc. London A,* **164,** 476.

P.D. Williams, T.W.N Haine, and P.L. Read (2008), Inertia-gravity waves emitted from balanced flow: observations, properties and consequences. *J. Atmos. Sci.,* **65,** 3543-3556.